

# The Magnetic Eden Model

Julián Candia<sup>a</sup> and Ezequiel V. Albano<sup>b</sup>

<sup>a</sup>*Center for Complex Network Research and Department of Physics,  
Northeastern University, Boston, MA 02115, USA*

Email address: jcandia@nd.edu

<sup>b</sup>*INIFTA, CCT La Plata, Universidad Nacional de La Plata,  
La Plata, Argentina*

Email address: ealbano@inifta.unlp.edu.ar

November 4, 2018

## Abstract

In the magnetic Eden model (MEM), particles have a spin and grow in contact with a thermal bath. Although Ising-like interactions affect the growth dynamics, deposited spins are frozen and not allowed to flip. This review article focuses on recent developments and future prospects, such as spontaneous switching phenomena, critical behavior associated with fractal, wetting, and order-disorder phase transitions, the equilibrium/nonequilibrium correspondence conjecture, as well as dynamical and critical features of the MEM defined on complex network substrates.

*Keywords:* Kinetic growth models; phase transitions; nonequilibrium processes; complex networks; sociophysics.

## 1 Introduction

Half a century ago, a seminal article by Murray Eden presented a stochastic kinetic model for the growth of bacterial colonies [1]. Except for a follow-up publication by the same author [2], this model went unnoticed for more than two decades, until it was rediscovered as the precursor (and probably the

simplest realization) of a large class of kinetic growth models that later drew huge attention in many areas of scientific research and technology.

Indeed, the Eden model and other kinetic growth models such as directed percolation, ballistic deposition, diffusion limited aggregation, random deposition with and without relaxation, cluster-cluster aggregation, etc., have been applied to a wide variety of phenomena: crystal and polycrystalline growth, molecular beam epitaxy, gelation, fracture propagation in solids, colloids, dielectrics, epidemic spreading, bacterial and fungi growth colonies, sedimentation, vapor deposition, wound healing and tissue regeneration, wetting and surface diffusion, etc. (for reviews, see, e.g., [3, 4, 5, 6, 7, 8, 9, 10, 11]). More recently, natural extensions to the Eden and other standard kinetic growth models have been proposed and studied: magnetic [12] and charged-particle Eden cluster growth [13], binary mixture growth with competition [14], magnetic diffusion-limited aggregation [15], magnetically controlled ballistic deposition [16], Cayley and diluted Cayley trees with two-state particles [17], etc.

In this context, this review article will focus on recent developments on the so-called magnetic Eden model (MEM), defined as an aggregate of particles with a magnetic moment coupled through Ising-like interactions. The system grows in contact with a thermal bath, but deposited spins are frozen and not allowed to flip. Hence, although the interaction configuration energy for MEM clusters is chosen to resemble the Ising Hamiltonian, the MEM is a model for irreversible growth under far-from-equilibrium conditions.

In regular lattices, the MEM's growth process leads to Eden-like self-affine growing interfaces and fractal cluster structures in the bulk [18, 19], and displays a rich variety of nonequilibrium phenomena, such as thermal order-disorder continuous phase transitions [20], spontaneous magnetization reversals [21], as well as morphological [22, 23], wetting [24, 25], and corner wetting transitions [26]. While the MEM was originally motivated by the study of structural properties of magnetically textured materials [12, 18], this model can also provide useful insight into kinetic phenomena of great experimental and theoretical interest, such as the growth of metallic multilayers [27] and thin films interacting with a substrate [28], fluid adsorption on wedges [29], filling of templates imprinted with nanometer/micrometer-sized features [30, 31], etc. The MEM was extensively studied in confined stripped geometries [32] that resemble, for instance, experiments on the growth of quasi-one-dimensional Fe strips on Cu(111) vicinal surfaces [33] and Fe on W(110) stepped substrata [34].

Despite the conceptual simplicity of its definition, this model displays a remarkably rich behavior and has a great potential for further applications, which prompted us to consider the MEM as a kind of “growing Ising model”.

Indeed, this is more than just a loose assertion: a quantitative correspondence between the critical behavior of the Ising model in  $d$  dimensions and the MEM in confined  $(d + 1)$ -dimensional stripped geometries was conjectured, based on measurements of order parameter probability distributions (for  $d = 1, 2$ ) and critical exponents [20]. Remarkably, similar correspondences between nonequilibrium two-state systems and the Ising model were independently found in other contexts [35, 36], suggesting an intriguing linkage between equilibrium and nonequilibrium systems yet to be better exploited and understood.

Following the increasing contribution of statistical physics to areas of interdisciplinary interest (for reviews, see, e.g., [37, 38, 39, 40]), the MEM was recently studied on small-world and scale-free network substrates as a socio-physical model for irreversible opinion spreading phenomena [41, 42, 43]. Indeed, physical concepts such as temperature and magnetization, spin growth and clustering, ferromagnetic-paramagnetic phase transitions, etc, can be meaningfully reinterpreted in sociological/sociophysical contexts. As expected, the MEM's dynamical and critical behavior is observed to depend very strongly on the topology of the substrate. Interestingly, however, similarities and differences are found when comparing the MEM to analogous equilibrium spin models.

The rest of the paper is laid out as follows. In Sect. 2, we define the model and outline a useful Monte Carlo simulation procedure. In Sect. 3, we provide a brief overview of the main findings about the MEM growing on regular lattice and complex network substrates. Finally, in Sect. 4 we state the conclusions and outlook.

## 2 The model: definition and simulation method

In the original Eden model, which is defined on a 2D square lattice, the growth process starts by adding particles to the immediate neighborhood (the perimeter) of a seed particle. Subsequently, particles are stuck at random to perimeter sites, leading to the formation of compact clusters with a self-affine interface. The model's behavior is robust, since the interface growth exponents are invariant under different seed geometries and different rules for the deposition process [44, 45, 46]. In fact, it is well established that the interface of the Eden model is described by the Kardar-Parisi-Zhang (KPZ) equation [47], similarly to other models that belong to the KPZ universality class [7, 10], such as, e.g., ballistic deposition.

Motivated by the observation of structural features in the magnetically textured growth of high critical-current density superconductors [48, 49],

the magnetic Eden model (MEM) was originally proposed in Ref. [12] as an extension of the Eden model, in which an additional degree of freedom represents the spin of the growing particles. Starting from a seed, growth takes place by adding, one by one, further spins to the perimeter of the growing cluster, taking into account the corresponding interaction energies. By analogy to the Ising model, the energy  $E$  of a configuration of spins is given by

$$E = -\frac{J}{2} \sum_{\langle ij \rangle} S_i S_j - \sum_i H_i S_i, \quad (1)$$

where  $S_i = \pm 1$  indicates the orientation of the spin for each occupied site (labeled by the subindex  $i$ ),  $J$  is the coupling constant between nearest-neighbor (NN) spins,  $H_i$  is the magnetic field applied on site  $i$ , and  $\langle ij \rangle$  indicates that the summation is taken over all pairs of occupied NN sites.

Setting the Boltzmann constant equal to unity ( $k_B \equiv 1$ ), the probability for a new spin to be added to the (already grown) cluster is defined as proportional to the Boltzmann factor  $\exp(-\Delta E/T)$ , where  $\Delta E$  is the resulting total energy change and  $T$  is the absolute temperature of the thermal bath<sup>1</sup>. Notice that, actually, the total energy change involves only the deposition site and its occupied nearest neighbors: the change in the spin-spin interaction term (i.e., the first term in Eq.(1)) just reflects the magnetic coupling between the already existing cluster and the newly added spin, while the change in the second term of Eq.(1) is simply given by the interaction between the new spin and the local magnetic field. At each step, all perimeter sites have to be considered and the probabilities of adding a new (either up or down) spin to each site must be evaluated. Using the Monte Carlo simulation method, all growth probabilities are first computed and normalized, and then the growing site and the orientation of the new spin are both determined by means of a pseudo-random number<sup>2</sup>. Let us point out again that, although Eq.(1) resembles the Ising Hamiltonian, the MEM is a nonequilibrium model in which new spins are continuously added, while older spins remain frozen and are not allowed to flip.

Figure 1 shows different setups that have already been considered: (a) planar substrates on the square lattice, (b)  $(d + 1)$ -dimensional confined (stripped) geometries, (c) small-world networks, and (d) scale-free networks. Up (down) spins are shown in red (black), empty sites in white. The typical Monte Carlo procedure requires performing averages over a large number of

---

<sup>1</sup>Energy, magnetic field, and temperature are measured here in units of the NN coupling constant,  $J$ , throughout.

<sup>2</sup>Fortran codes with Monte Carlo implementations of the MEM under different setups are freely available from the authors upon request.

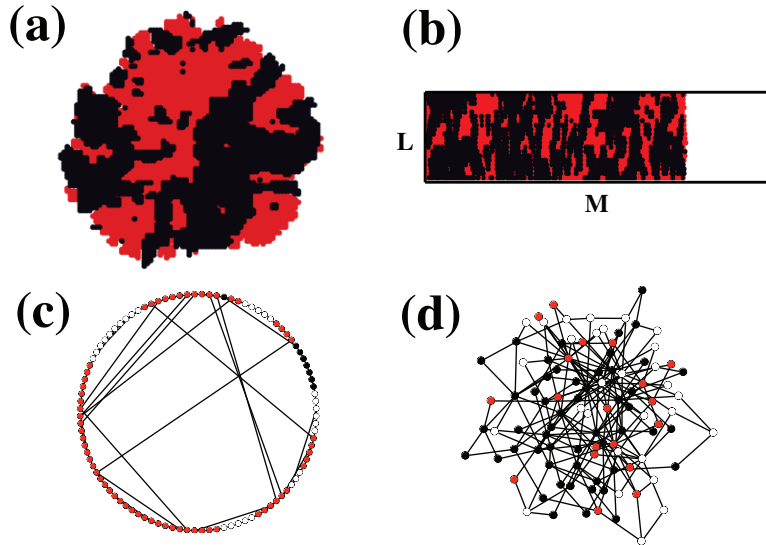


Figure 1: MEM growth under different setups: (a) planar substrates on the square lattice, (b)  $(d+1)$ -dimensional confined (stripped) geometries, (c) small-world networks, and (d) scale-free networks. Red (black) sites represent up (down) spins, while empty sites are shown in white.

statistical ensembles generated under the same conditions (i.e., temperature, magnetic fields, NN couplings, etc). For complex network substrates, ensemble averages over different (but topologically equivalent) network realizations are necessary as well.

Note that the substrate geometry naturally suggests the seed to be chosen. For planar substrates (Figure 1(a)), a single spin originates unconfined clusters (which, growing on the square lattice, acquire a diamond shape [50]). For  $L^d \times M$  stripped geometries with  $L \ll M$  (Figure 1(b)), linear/planar transversal seeds lead to longitudinal growth. For small-world (Figure 1(c)) and scale-free (Figure 1(d)) networks, growth from single spin seeds naturally stops once the system becomes completely filled.

Allowing the MEM to grow under different conditions, a remarkably rich variety of growth phenomena is encountered. Indeed, different growth modes arise from using confined and unconfined geometries, varying the dimensionality of the substrate, considering positive and negative coupling constants, applying surface and bulk magnetic fields (which can also be spatially homogeneous, periodic or random), changing the topology of the substrate, etc. Some of these phenomena were recently uncovered and will be summarized in the next section. Yet, a horizon of exciting new possibilities for the MEM applied to fields as different as materials science, biophysics, and sociophysics

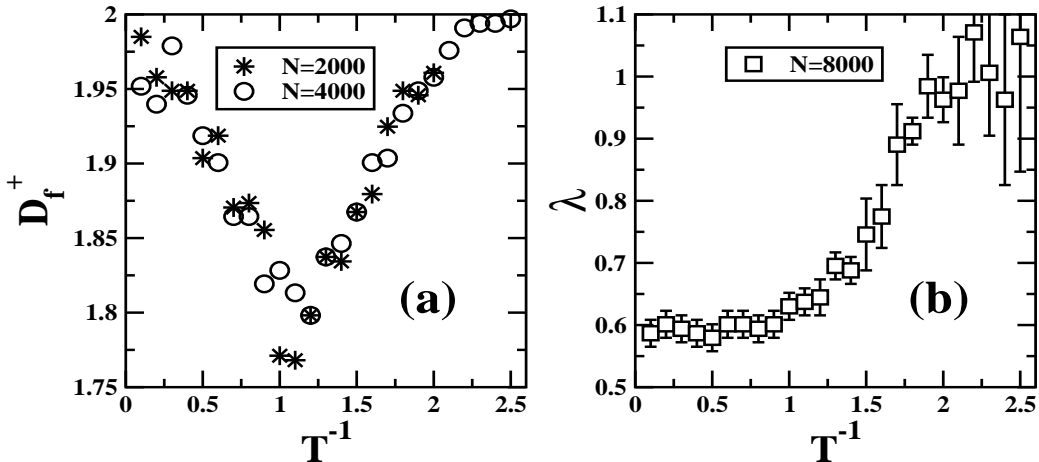


Figure 2: Geometrical transitions for the MEM growing on 2D planar substrates: (a) fractal dimension of the up component versus temperature, and (b) lacunarity exponent versus temperature (adapted from Ref. [18]).

can be envisioned.

### 3 Overview of main results

#### 3.1 Unconfined geometries: Lacunarity, fractal and magnetic pseudophase transitions

The 1D MEM growing from a single seed can be solved exactly and leads to a thermal order-disorder pseudophase transition taking place at a finite “critical temperature”  $T_c(N)$ , which is weakly dependent upon the system size  $N$ . However, since  $T_c^{-1} \sim \log(N)$ , the system is noncritical in the ( $N \rightarrow \infty$ ) thermodynamic limit [12]. A similar scaling behavior was also reported for the MEM growing on unconfined 2D planar substrates (Figure 1(a)). Interestingly, however, these finite-size, order-disorder “phase transitions” are well correlated to geometrical transitions associated with fractal and lacunar structures in the bulk [18, 19].

The fractal dimension  $D_f^+$  of the up species can be measured by counting the number  $n^+$  of up spins in boxes of different sizes  $\epsilon$  centered on the seed site, i.e.,

$$n^+ \sim \epsilon^{D_f^+}, \quad (2)$$

a method originally used to obtain the fractal dimension of smoke aggregates [51]. Figure 2(a) shows a clear departure of  $D_f^+$  from the Euclidean space

dimension of the substrate,  $D = 2$ , with a sharp minimum equal to  $D_f^+ = 1.79 \pm 0.03$  at the “critical” temperature  $T_c^{-1} = 1.2 \pm 0.1$  (for  $N = 4000$ ) [18].

The lacunarity density,  $l_d$ , is defined as the total number of empty sites enclosed in the bulk by occupied neighbors, normalized by the total number of deposited spins  $N$ . For the Eden model, the lacunarity density obeys the scaling law

$$l_d \sim N^{\lambda-1}, \quad (3)$$

with  $\lambda = 0.56 \pm 0.01$ . For the MEM, however, the lacunarity exponent depends on the temperature and undergoes a transition towards unity at  $T \approx T_c$  [18]. Figure 2(b) shows the thermal dependence of the lacunarity exponent for a system of size  $N = 8000$ .

### 3.2 Confined stripped geometries: spontaneous switching, phase transitions and the equilibrium / nonequilibrium correspondence conjecture

At low temperatures, magnetic Eden films grown on a stripped geometry of finite linear dimension  $L$  (Figure 1(b)) display *spontaneous magnetization reversals*: a sequence of well-ordered magnetic domains separated by abrupt collective spin reversals of characteristic length  $l_R \sim L$ <sup>3</sup>[21] (see Figure 3). This phenomenon is due to thermal fluctuations on the finite-size thin films. Indeed, although at low temperatures the bulk grows in an ordered state, sizable fluctuations may occur, eventually driving the finite-size system across a drastic magnetization reversal.

The probability of occurrence of spontaneous magnetization reversals vanishes as the system’s linear size tends to the ( $L \rightarrow \infty$ ) thermodynamic limit. However, this mechanism is relevant for many real mesoscopic systems, since clearly such spontaneous (and, thus, uncontrollable) reversals must be avoided in the preparation of high-quality magnetic thin films and nanowires. These shortcomings may disappear if the film strongly interacts with the substrate where the actual growing process takes place, as modeled, for instance, by surface and/or bulk fields that could account for the interaction with the substrate or with externally applied magnetic fields.

The degree of order in a magnetic system can be naturally characterized by the ensemble-averaged magnetization per site. In the case of  $(d + 1)$ -dimensional stripped geometries, the magnetization is averaged over the transversal direction (e.g., transversal columns of  $L$  spins for  $d = 1$ , and

---

<sup>3</sup> Notice that, since we consider  $L \times M$  strips with  $L \ll M$ , the longitudinal direction is effectively infinite and  $L$  is the only relevant linear scale in the substrate.

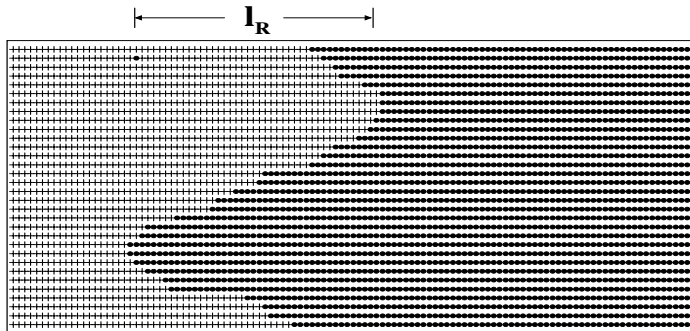


Figure 3: Spontaneous magnetization reversal in a  $(1+1)$ -dimensional magnetic thin film. The snapshot corresponds to the bulk of the sample and the growing interface is not shown.

transversal planes of  $L \times L$  spins for  $d = 2$ ), i.e.,

$$m = \left\langle \frac{1}{L^d} \sum S_i \right\rangle. \quad (4)$$

The thermal dependence of the order parameter probability distributions,  $P_L(m)$ , contains information about all momenta of the order parameter  $m$ , including universal ratios such as the Binder cumulant [52]. Figure 4 shows plots of  $P_L(m)$  versus  $m$  for different values of temperature, substrate dimension and linear size: (a)  $d = 1, L = 128$ ; and (b)  $d = 2, L = 16$ . In both cases, the high- $T$  distributions are peaked at  $m = 0$  and can be well approximated by Gaussian distributions. However, as temperature decreases, their behavior is fundamentally different. In the  $d = 1$  case, the distribution broadens and develops two peaks at  $m = \pm 1$ , which become dominant while the distribution turns distinctly non-Gaussian, with an absolute minimum at  $m = 0$ . In sharp contrast, by lowering the temperature in the  $d = 2$  case the distribution develops two symmetrical maxima located at  $m = \pm M_{sp}$  ( $0 < M_{sp} < 1$ ), which become steeper and approach  $m = \pm 1$  as  $T$  decreases further.

This behavior bears close resemblance to the order parameter probability distributions of the  $d$ -dimensional Ising model [53, 54], suggesting a non-trivial connection between the critical behavior of the  $(d+1)$ -dimensional MEM and the Ising model in  $d$  dimensions (see [20] for a full discussion). For  $d = 1$ , the ordered phase is trivially found only at  $T = 0$ , while for  $d = 2$ , MEM films exhibit a continuous order-disorder phase transition at the critical temperature  $T_c = 0.69 \pm 0.01$ . This connection can indeed be further confirmed by measurements of critical exponents in the  $d = 2$  case. Using standard finite-size scaling analysis [55, 56], the MEM's critical exponents



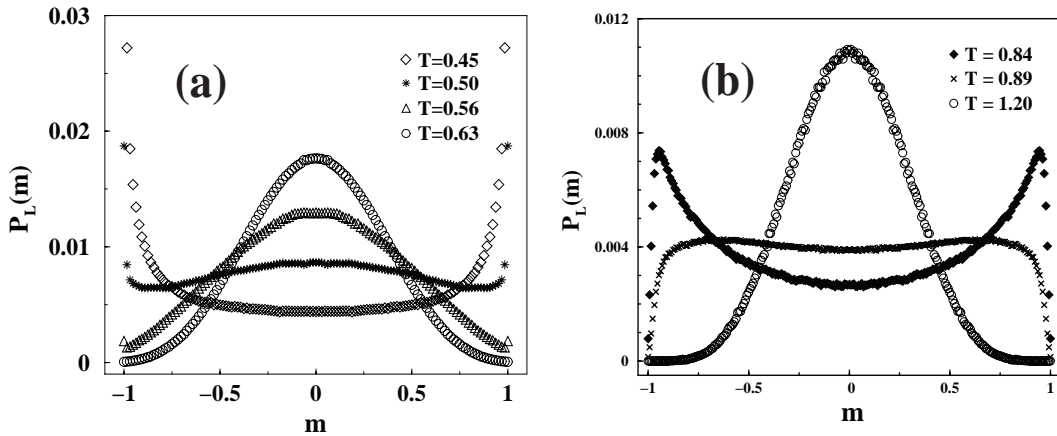


Figure 4: Order parameter probability distributions for different temperatures and substrates: (a)  $d = 1, L = 128$ ; (b)  $d = 2, L = 16$ . In (a), the sharp peaks at  $m = \pm 1$  for  $T = 0.45$  have been truncated.

are found:  $\nu = 1.04 \pm 0.16$ ,  $\gamma = 2.10 \pm 0.36$ , and  $\beta = 0.16 \pm 0.05$ , which agree well within error bars with the exact critical exponents for the Ising model in 2 dimensions:  $\nu = 1$ ,  $\gamma = 7/4$ , and  $\beta = 1/8$ .

It is interesting to point out that similar connections between nonequilibrium systems and the Ising model were independently found in other contexts. For  $d$ -dimensional probabilistic cellular automata with two states and up-down symmetry, it was shown that if the system undergoes a symmetry breaking, its critical behavior is identical to the corresponding Ising model in equilibrium [35]. Furthermore, studies on thin film  $(d + 1)$ -dimensional binary alloys with surface equilibration (but such that atoms in the bulk are frozen) show that the behavior parallel to the growth direction reflects the dynamics of an Ising system in  $d$  dimensions [36]. These findings suggest an intriguing linkage between equilibrium and nonequilibrium systems that should be further exploited and understood, and the MEM offers an open avenue to gain deeper insight into this issue.

Certainly, the validity of this conjecture could be further confirmed (or, for that sake, otherwise ruled out) by performing more accurate and complete numerical studies that may narrow down error bars and explore other critical exponents. In the same vein, the exploration of higher dimensional systems (i.e.,  $d \geq 3$ ) would contribute to this goal. However, MEM's growth rules require updating the growth probabilities at each time step and lead to very slow algorithms compared to analogous equilibrium spin models. An alternative path is the search for analytic solutions, so far only known for the  $d = 1$  semiopen chain [12].

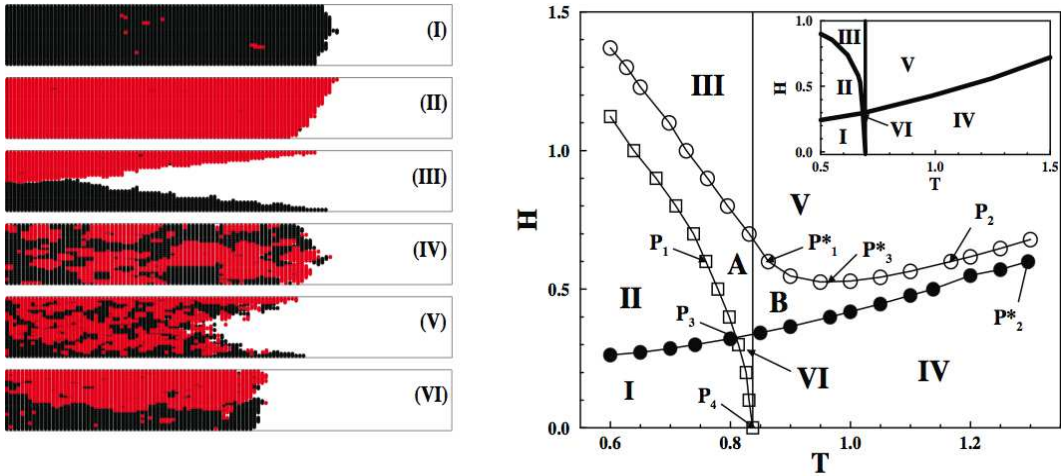


Figure 5: Bulk and interfacial phase transitions in  $L^2 \times M$  thin films. The left panel shows longitudinal slice snapshots for  $L = 32$  and different temperatures and surface magnetic fields: (I)  $H = 0.05$ ,  $T = 0.6$ ; (II)  $H = 0.5$ ,  $T = 0.55$ ; (III)  $H = 1.4$ ,  $T = 0.6$ ; (IV)  $H = 0.1$ ,  $T = 1.0$ ; (V)  $H = 1.6$ ,  $T = 1.4$ ; and (VI)  $H = 0.20$ ,  $T = 0.82$ . The right panel shows the  $H - T$  phase diagram for  $L = 12$ , as well as the extrapolation to the thermodynamic limit (inset).

Interfacial phase transitions and critical phenomena in confined samples exhibit a quite distinct physical behavior compared to that occurring in the bulk due to the finite separation between the walls and the specific wall-particle interaction [57]. When competing short-range magnetic fields are applied to the upper and lower surfaces along the longitudinal direction, MEM films exhibit different kinds of growth mode and lead to a rich phase diagram on the  $H$  versus  $T$  plane (see [25] for a full discussion). Indeed, the interplay between confinement and growth mode leads to a localization-delocalization transition in the interface that runs along the walls and a change of the curvature of the growing interface running perpendicularly to the walls. Extrapolation of this scenario to the thermodynamic limit leads to a multicritical wetting transition under far-from equilibrium conditions. It is worth mentioning that the study of out of equilibrium wetting phenomena has also attracted considerable attention in a context related to the evolution of growing interfaces [58, 59, 60].

The occurrence of different growth modes is evident in the snapshot configurations on the left panel of Figure 5, where longitudinal slices of  $L^2 \times M$  films ( $M \gg L$ ) are shown for different temperatures and surface magnetic fields. As above discussed, thermally driven transitions in the bulk separate

the low- $T$  ordered regime (phases I, II, III, and VI) from the high- $T$  disordered one (phases IV and V). Moreover, a wetting localization-delocalization phase transition (associated with the longitudinal interface between up and down domains) takes place within the ordered-bulk phase, separating the nonwet region (phases I and II) from the wet region (phases III and VI). Finally, due to the so-called missing neighbor effect and varying intensity of wall-particle interactions, different contact angles and curvatures in the *growing* interface (i.e., the transverse interface between occupied and empty lattice sites) are also observed. These wetting-like, morphological transitions separate distinct growth regimes, characterized by either convex (phases I and IV), nondefined (phases II and VI), or concave (phases III and V) growing interfaces.

Standard procedures allow quantifying these phenomena, leading to the rich phase diagrams shown on the right panel of Figure 5. For finite-size systems, two additional regions (labeled  $A$  and  $B$ ) are observed, although they just represent intermediate states that cannot be associated with distinct physical processes. By extrapolating to the thermodynamic limit, regions  $A$  and  $B$  shrink and vanish, leading to the phase diagram shown in the inset. In different geometrical settings, such as, e.g., growth on wedges [26], other interesting interfacial phase transition phenomena are observed (not discussed here for the sake of space).

### 3.3 Complex networks: dynamics and criticality of opinion spreading phenomena

As part of the increasing application of statistical physics to interdisciplinary fields of science, a variety of Ising-like spin models have been recently studied in the context of sociophysical phenomena (see, e.g., [61, 62, 63, 64, 65, 66, 67, 68]). Under this interpretation, spin states denote different opinions or preferences, while the coupling constant describes the convincing power between interacting individuals, which is in competition with the “free will” represented as thermal noise [65]. In particular, much attention has been devoted to spin models defined on complex networks, since the underlying complex network topology of the substrate reflects some key aspects of social structures, such as the small-world effect and the high connectivity of local neighborhoods [69, 70, 71, 72].

In this context, the MEM has been recently studied on small-world and scale-free network substrates as a sociophysical model for irreversible opinion spreading phenomena [41, 42, 43]. According to the MEM’s rules, the opinion or decision of an individual is affected by those of his or her acquaintances,

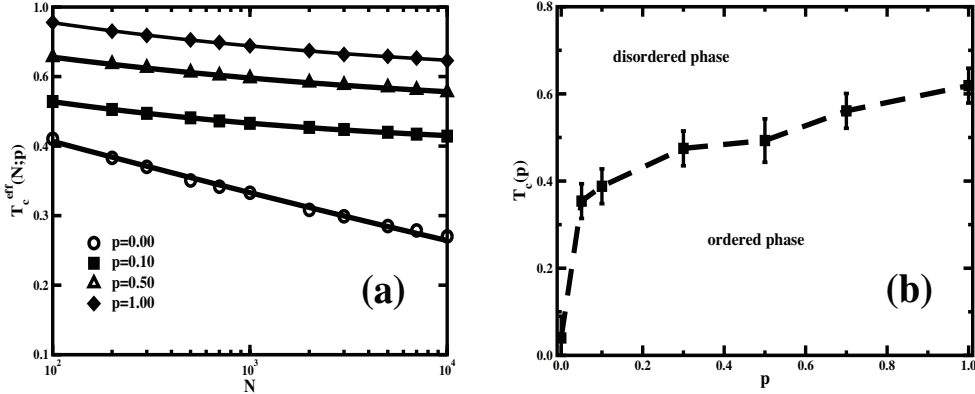


Figure 6: (a) Effective transition temperatures for the MEM growing on 1D SWNs of size  $10^2 \leq N \leq 10^4$  and different values of  $p$  (symbols), and fits to the data (solid lines) using the finite-size scaling relation, Eq.(5). (b) Phase diagram  $T_c(p)$  versus  $p$  corresponding to  $N \rightarrow \infty$ .

but opinion changes (analogous to spin flips in an Ising-like model) do not occur. Hence, as opposed to equilibrium spin models, the MEM could be applied to sociological scenarios in which individuals are subject to highly polarized, short term, binary choice situations. Given these conditions opinions are not expected to fluctuate and “thermalize”. One example is a binary voting scenario, such as a ballottage or referendum, where model predictions could be empirically tested using time-resolved data from polls and surveys.

The MEM was studied on two paradigmatic types of complex network: (a) the nearest-neighbor, adding-type small-world network (SWN) [73, 74], which is built by randomly adding new links onto an underlying ordered lattice (for each bond in the original lattice, a shortcut is added with probability  $p$ ); (b) Barabási-Albert (BA) and uncorrelated scale-free (SF) networks, which are characterized by power-law degree distributions, i.e.,  $P(k) \sim k^{-\gamma}$ . BA networks are built by following the preferential attachment growth mechanism: a new node with  $m$  edges is added at every time step and is connected to  $m$  different nodes already present in the system. The probability for an already existing node to acquire a new link is proportional to that node’s degree [70, 75]. Instead, uncorrelated SF networks arise from pairwise connecting link ends, which are chosen according to a power-law distribution [70, 71]. The degree exponent for BA networks is  $\gamma_{BA} = 3$ , while in the case of uncorrelated SF networks,  $\gamma$  is a free parameter.

The symbols in Figure 6(a) show effective transition temperatures,  $T_c^{eff}(N; p)$ , which separate the ordered regime from the disordered one for the MEM growing on 1D SWNs of different size and shortcut-adding probabilities. Fits to the data are also shown (solid lines), as obtained from the finite-size scaling relation

$$|T_c(p) - T_c^{eff}(N; p)| \propto N^{-1/\nu}, \quad (5)$$

where  $T_c(p)$  is the true  $p$ -dependent critical temperature (corresponding to  $N \rightarrow \infty$ ) and  $\nu$  is the exponent that characterizes the divergence of the correlation length at criticality. In Figure 6(b), the phase diagram  $T_c(p)$  versus  $p$  shows the critical behavior of the system in the thermodynamic limit. For  $p > 0$ , the MEM undergoes critical order-disorder phase transitions at finite critical temperatures: the small-world network geometry triggers criticality. Naturally, the weaker the global order imposed by long-range shortcuts, the lower the shortcut fraction, and hence  $T_c(p)$  decreases monotonically with  $p$ . Moreover, the critical temperature is observed to vanish for  $p = 0$ , which is the expected regular lattice limit behavior.

The same fits of Eq.(5) to the numerical data also determine the critical exponent  $\nu$ . The obtained ( $p$ -independent) value is  $\nu = 3.6 \pm 0.4$ . As in the case of equilibrium spin systems defined on small-world networks (see, e.g., [64, 67]), the universality class of this nonequilibrium system is not observed to depend on the shortcut density, provided that  $p > 0$ . An additional characterization of the critical behavior of the MEM defined on 1D SWNs can be obtained by calculating the critical exponent  $\gamma$ , which describes the divergence of the susceptibility at the critical point. The exponent ratio  $\gamma/\nu$  can be related to the peak of the susceptibility measured in finite samples of size  $N$  by [56]

$$\chi_{max} \propto N^{\gamma/\nu}. \quad (6)$$

It turns out that  $\gamma/\nu = 0.92 \pm 0.04$ , and hence  $\gamma = 3.3 \pm 0.4$ .

The onset of criticality induced by the presence of long-range connections is also observed when the MEM grows on 2D SWNs [43]. The underlying 2D substrate, however, allows observing other phenomena of interest, such as the collision of different shortcut-induced opinion fronts, domain growth and cluster formation. The formation of rich domain structures, which depends on both the temperature and the shortcut distribution, can be characterized quantitatively by measurements such as the cluster size probability distribution, the size of the largest cluster, and the number of different clusters. Figure 7 shows the cluster size probability distribution and the mean number of different clusters for a system of size  $N = 10^4$  and different values of shortcut-adding probability and temperature.

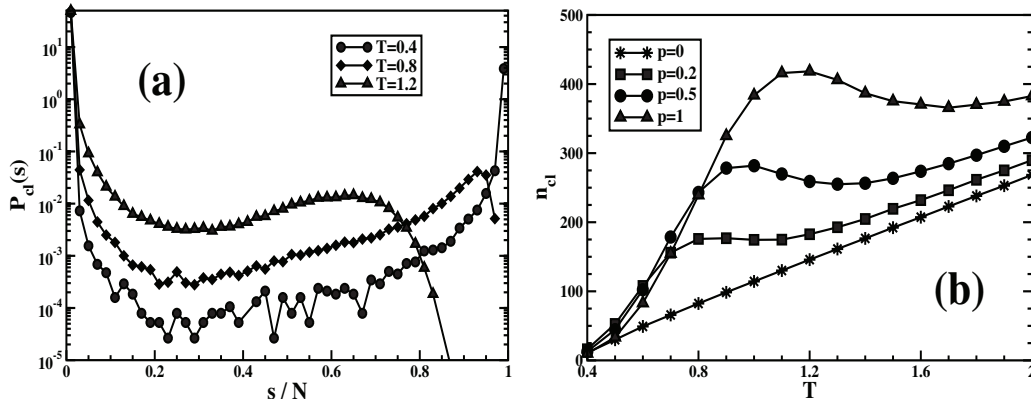


Figure 7: Domain structure for the MEM growing on 2D SWNs of size  $N = 10^4$  and different values of shortcut-adding probability and temperature: (a) cluster size probability distribution (for  $p = 0.5$ ); (b) mean number of different clusters.

The probability of occurrence of a cluster of size  $s$ ,  $P_{cl}(s)$ , is shown in Figure 7(a) for  $p = 0.5$  and different temperatures, as indicated. Due to thermal fluctuations, all distributions show an absolute maximum at small cluster sizes ( $s/N \ll 1$ ). However, the probability distribution for large clusters reveals intrinsic differences in the growth mode, which depend on the temperature. Apart from statistical fluctuations, the distributions of clusters of size  $s/N \geq 0.2$  grow monotonically with  $s$ . However, for  $T = 0.4$ , the monotonic trend continues up to  $s/N = 1$ , where the distribution has a local maximum, while for larger temperatures, the distributions show abrupt cutoffs at  $s/N < 1$ , the more evident, the larger the temperature. Figure 7(b) shows the thermal dependence of the mean number of different clusters,  $n_{cl}$ . The  $p > 0$  plots show broad local maxima taking place at intermediate temperatures. As with response functions such as the susceptibility and heat capacity, the observed maxima are indicative of peak fluctuations in the cluster structure due to thermally driven, bulk order-disorder phase transitions. Indeed, following a procedure analogous to that described above for 1D SWNs, one can characterize the critical behavior of the system in the thermodynamic limit (see [43] for more details).

Contrary to the case of SWNs, SF networks provide an interesting setting in which the social roles differ significantly from one agent to another. In particular, hubs in the SF network represent highly influential individuals,

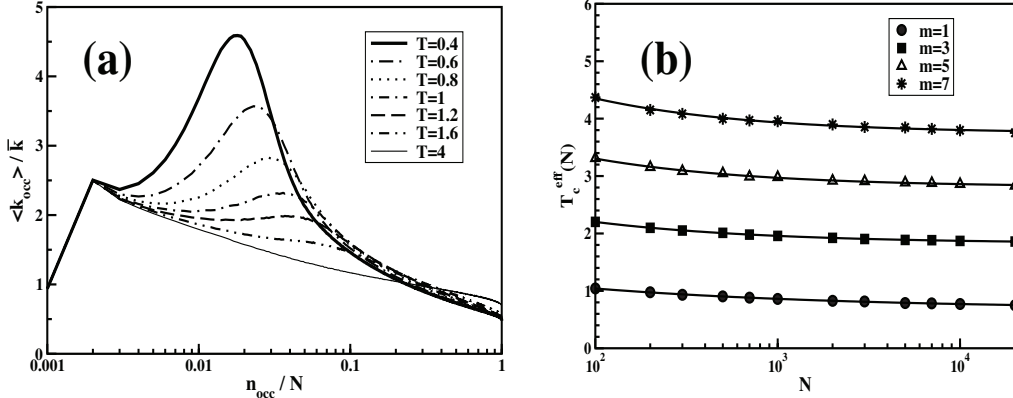


Figure 8: (a) Average degree of occupied nodes for the MEM growing on BA networks of size  $N = 10^3$ ,  $m = 3$ , and different temperatures, as a function of the fraction of deposited particles,  $n_{occ}/N$ . (b) Effective transition temperatures corresponding to BA networks of different sizes and values of the parameter  $m$  (symbols), and finite-size scaling fits (solid lines).

whose opinions can potentially affect the decisions of many other individuals in the society. Let us first discuss the dynamical behavior of MEM clusters growing on finite BA scale-free networks.

The process of spin deposition (or, equivalently, opinion spreading) can be characterized by computing the degree of the newly occupied node,  $k_{occ}$ , each time a new particle is added to the system. Figure 8(a) shows the average degree of occupied nodes relative to the network's mean degree,  $\langle k_{occ} \rangle / \bar{k}$ , for BA networks of size  $N = 10^3$ ,  $m = 3$ , and different temperatures, as a function of the fraction of occupied nodes,  $n_{occ}/N$ . Since at low temperatures the system tends to develop highly ordered spin domains, highly connected nodes have larger probabilities to be occupied at early times during the growth process. The leading role of hubs is clearly observed in the low-temperature plots of Figure 8(a), where  $\langle k_{occ} \rangle / \bar{k} \gg 1$  at early stages of the growth process, i.e., when the number of occupied nodes is of the order of a few percent of the total system size. At higher temperatures, however, the increased thermal noise tends to wash out the phenomenon of *preferential spin deposition*. The growth at later times mainly proceeds by the occupation of less-than-average connected nodes, which leads to roughly  $T$ -independent values of  $\langle k_{occ} \rangle$ .

The critical behavior of the system, as follows from the standard finite-size scaling procedures discussed above, is depicted in Figure 8(b). The effective

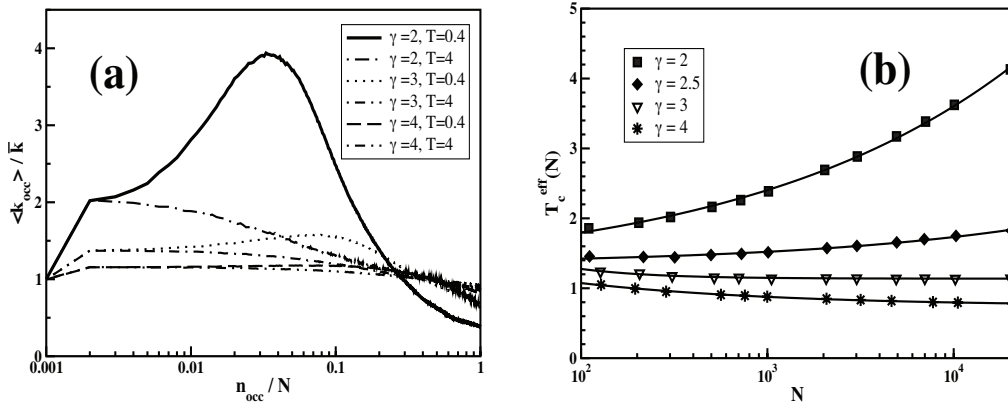


Figure 9: (a) Average degree of occupied nodes for uncorrelated SF networks of size  $N \approx 10^3$ , minimum degree  $k_0 = 3$ , and different values of temperature and degree exponent. (b) Effective transition temperatures for uncorrelated SF networks (with  $k_0 = 3$ ) as a function of size and degree exponent (symbols), along with finite-size scaling fits (solid lines).

pseudocritical temperatures decrease monotonically with the network size and lead to finite extrapolations in the thermodynamic limit. The monotonic increase of  $T_c(m)$  can be well approximated by the linear relation  $T_c(m) = 0.522(3) \times m + 0.21(1)$ , while the exponent  $\nu$  decreases monotonically and tends to  $\nu \approx 2$  for  $m \geq 3$ .

Finally, let us consider the irreversible growth of MEM clusters on uncorrelated SF networks, which allow a free choice of the degree exponent  $\gamma$ . Figure 9(a) shows  $\langle k_{occ} \rangle / \bar{k}$  versus  $n_{occ} / N$  for uncorrelated SF networks generated with different values of  $\gamma$  and for different temperatures, as indicated. The phenomenon of preferential spin deposition, due to the dominant role played by hubs during the early stages of the growth process, is only significant at low temperatures. Moreover, this phenomenon is observed to be relevant only for low degree exponents  $\gamma < 3$ . Since the preferential spin deposition is a feature associated with the formation of large ordered clusters during the growth process, these results agree well, at a qualitative level, with the analogous behavior reported for the Ising model on uncorrelated scale-free networks [68], in which the disorder was observed to grow monotonically with the exponent  $\gamma$ .

Figure 9(b) shows the effective transition temperatures for uncorrelated SF networks of minimum degree  $k_0 = 3$ , for different values of network size



and the degree exponent. The critical behavior turns out to be crucially dependent on the steepness of the degree distribution: while for  $\gamma \geq 3$ , the trend is similar to the behavior observed for BA networks, the plots corresponding to smaller values of  $\gamma$  are observed to diverge, hence implying the absence of paramagnetic-ferromagnetic phase transitions in the thermodynamic limit.

Using finite-size scaling procedures, one finds  $T_c = 1.14(2)$  and  $\nu = 0.9(1)$  (for  $\gamma = 3$ ), and  $T_c = 0.74(1)$  and  $\nu = 2.6(2)$  (for  $\gamma = 4$ ). Comparing these observations with the results reported for the Ising model on uncorrelated scale-free networks [68], we find a qualitative agreement for both  $\gamma < 3$  (i.e., the absence of a paramagnetic phase in the thermodynamic limit) and  $\gamma > 3$  (i.e., the existence of a finite critical temperature delimiting the paramagnetic-ferromagnetic phase transition). Instead, the convergence of the critical temperature for the  $\gamma = 3$  case is clearly in contrast with the logarithmic divergence observed in the Ising model.

## 4 Conclusions and Outlook

The magnetic Eden model (MEM) is a kinetic growth model in which particles have a spin and grow in contact with a thermal bath. Although Ising-like interactions affect the growth dynamics, deposited spins are frozen and not allowed to flip. This model describes nonequilibrium binary mixture growth phenomena that have a wide range of potential applications in contexts as different as materials science, sociophysics, and biophysics.

In regular lattices, the MEM's growth process leads to Eden-like self-affine growing interfaces and fractal cluster structures in the bulk, and displays a rich variety of nonequilibrium phenomena, such as thermal order-disorder continuous phase transitions, spontaneous magnetization reversals, as well as morphological, wetting, and corner wetting transitions.

In a sense, the MEM can be regarded as a “growing Ising model”, and indeed a quantitative correspondence between the critical behavior of the Ising model in  $d$  dimensions and the MEM in confined  $(d + 1)$ -dimensional stripped geometries was conjectured, based on measurements of order parameter probability distributions and critical exponents. Certainly, further work in this direction is needed to gain further understanding of this correspondence, which suggests an intriguing linkage between equilibrium and nonequilibrium systems. Remarkably, similar connections between nonequilibrium two-state systems and the Ising model were independently found in other contexts.

Very recently, the MEM has also been investigated on complex network substrates such as small-world and scale-free networks. Interpreted as a

sociophysical model for irreversible opinion spreading phenomena, the MEM offers a complementary view of sociological processes studied by means of other spin models, and it could be applied to scenarios in which individuals are subject to highly polarized, short-term, binary choice situations, such as a ballottage or referendum. Other applications in this area may also include marketing campaigns, in which the influence of advertising could be modeled by externally applied fields.

This review summarizes the main results obtained so far on the MEM, with a bias towards the most recent work and applications, as well as discussions on open questions and outlook. Hopefully, growing research efforts on the MEM will follow, stimulating and contributing to further developments in the fields of nonequilibrium statistical physics, complex networks, and interdisciplinary science.

## Acknowledgments

This work is partially supported by CONICET, ANPCyT, and UNLP (Argentina). J. C. is supported by the James S. McDonnell Foundation and the National Science Foundation ITR DMR-0426737 and CNS-0540348 within the DDDAS program.

## References

- [1] M. Eden, *Symposium on Information Theory in Biology*, H. P. Yockey (Ed.) (Pergamon Press, New York, 1958), 359.
- [2] M. Eden, *Proc. 4th Berkeley Symposium on Mathematical Statistics and Probability*, F. Neyman (Ed.) (University of California Press, Berkeley, 1961), Vol.IV, 223.
- [3] H. J. Herrmann, *Phys. Rep.* **136**, 153 (1986).
- [4] F. Family and T. Vicsek, *Dynamics of Fractal Surfaces* (World Scientific, Singapore, 1991).
- [5] A. Bunde and S. Havlin (Eds.), *Fractals and Disordered Media* (Springer-Verlag, Heidelberg, 1991).
- [6] A. Bunde and S. Havlin (Eds.), *Fractals in Science* (Springer-Verlag, Heidelberg, 1995).

- [7] A.-L. Barabási and H. Stanley, *Fractal Concepts in Surface Growth* (Cambridge University Press, Cambridge, 1995).
- [8] M. Marsili, A. Maritan, F. Toigo, and J.R. Banavar, *Rev. Mod. Phys.* **68**, 963 (1996).
- [9] M. Eden and P. Thévenaz, *Proc. 6th Int. Workshop on Digital Image Processing and Computer Graphics (DIP'97)*, E. Wenger and L. Dimitrov (Eds.), SPIE Vol. 3346, 43 (1997).
- [10] H. Hinrichsen, *Adv. Phys.* **49**, 815 (2000).
- [11] G. Ódor, *Rev. Mod. Phys.* **76**, 663 (2004).
- [12] M. Ausloos, N. Vandewalle, and R. Cloots, *Europhys. Lett.* **24**, 629 (1993).
- [13] Y. V. Ivanenko, N. I. Lebovka, and N. V. Vygornitskii, *Eur. Phys. J. B* **11**, 469 (1999).
- [14] Y. Saito and H. Müller-Krumbhaar, *Phys. Rev. Lett.* **74**, 4325 (1995).
- [15] N. Vandewalle and M. Ausloos, *Phys. Rev. E* **51**, 597 (1995).
- [16] K. Trojan and M. Ausloos, *Physica A* **326**, 492 (2003).
- [17] N. Vandewalle and M. Ausloos, *J. Phys. A: Math. and Gen.* **29**, 7089 (1996).
- [18] N. Vandewalle and M. Ausloos, *Phys. Rev. E* **50**, R635 (1994).
- [19] M. Ausloos, N. Vandewalle, and R. Cloots, *J. Magn. Magn. Mater.* **140**, 2185 (1995).
- [20] J. Candia and E. V. Albano, *Phys. Rev. E* **63**, 066127 (2001).
- [21] J. Candia and E. V. Albano, *J. Appl. Phys.* **90**, 5395 (2001).
- [22] J. Candia and E. V. Albano, *J. Chem. Phys.* **117**, 6699 (2002).
- [23] J. Candia and E. V. Albano, *J. Phys.: Cond. Matt.* **14**, 4927 (2002).
- [24] J. Candia and E. V. Albano, *Eur. Phys. J. B* **16**, 531 (2000).
- [25] J. Candia and E. V. Albano, *Phys. Rev. Lett.* **88**, 016103 (2002).
- [26] V. Manías, J. Candia, and E. V. Albano, *Eur. Phys. J. B* **47**, 563 (2005).

- [27] U. Bovensiepen, F. Wilhelm, P. Srivastava, P. Pouloupoulos, M. Farle, A. Ney, and K. Baberschke, *Phys. Rev. Lett.* **81**, 2368 (1998).
- [28] M. Kulawik, N. Nilius, and H.-J. Freund, *Phys. Rev. Lett.* **96**, 036103 (2006).
- [29] K. Rejmer, S. Dietrich, and M. Napiórkowski, *Phys. Rev. E* **60**, 4027 (1999).
- [30] D. Josell, D. Wheeler, W. H. Huber, and T. P. Moffat, *Phys. Rev. Lett.* **87**, 16102 (2001).
- [31] A. De Virgiliis, O. Azzaroni, R. C. Salvarezza, and E. V. Albano, *Appl. Phys. Lett.* **82**, 1953 (2003).
- [32] J. Candia and E. V. Albano, *J. Magn. Magn. Mater.* **260**, 338 (2003).
- [33] J. Shen, R. Skomski, M. Klaua, H. Jenniches, S. Sundar Manoharan, and J. Kirschner, *Phys. Rev. B.* **56**, 2340 (1997).
- [34] O. Pietzsch, A. Kubetzka, M. Bode, and R. Wiesendanger, *Phys. Rev. Lett.* **84**, 5212 (2000).
- [35] G. Grinstein, C. Jayaprakash, and Y. He, *Phys. Rev. Lett.* **55**, 2527 (1985).
- [36] B. Drossel and M. Kardar, *Phys. Rev. E* **55**, 5026 (1997).
- [37] S. M. de Oliveira, P. M. C. de Oliveira, and D. Stauffer, *Non-Traditional Applications of Computational Statistical Physics* (B.G. Teubner, Stuttgart, 1999).
- [38] W. Weidlich, *Sociodynamics: a Systematic Approach to Mathematical Modelling in the Social Sciences* (Harwood Academic Publishers, Amsterdam, 2000).
- [39] D. Stauffer, S. M. de Oliveira, P. M. C. de Oliveira, and J. S. Sa Martins, *Biology, Sociology, Geology by Computational Physicists* (Elsevier, Amsterdam, 2006).
- [40] C. M. Bordogna and E. V. Albano, *J. Phys.: Condens. Matter* **19**, 065144 (2007).
- [41] J. Candia, *Phys. Rev. E* **74**, 031101 (2006).
- [42] J. Candia, *Phys. Rev. E* **75**, 026110 (2007).

- [43] J. Candia, J. Stat. Mech. P09001 (2007).
- [44] R. Jullien and R. Botet, J. Phys. A: Math. Gen. **18**, 2279 (1985).
- [45] P. Freche, D. Stauffer, and H. E. Stanley, J. Phys. A: Math. Gen. **18**, L1163 (1985).
- [46] R. Hirsch and D. E. Wolf, J. Phys. A: Math. Gen. **19**, L251 (1986).
- [47] M. Kardar, G. Parisi, and Y.-C. Zhang, Phys. Rev. Lett. **56**, 889 (1986).
- [48] C. Hannay, R. Cloots, and M. Ausloos, Solid State Commun. **83**, 349 (1992).
- [49] R. Cloots, A. Rulmont, C. Hannay, P. A. Godelaine, H. W. Vander-schueren, P. Régnier, and M. Ausloos, Appl. Phys. Lett. **61**, 2718 (1992).
- [50] M. T. Batchelor and B. I. Henry, Phys. Lett. A **157**, 229 (1991).
- [51] S. R. Forrest and T. A. Witten, J. Phys. A: Math. Gen. **12**, L109 (1979).
- [52] K. Binder, Z. Phys. B **43**, 119 (1981).
- [53] L. D. Landau and E. M. Lifshitz, *Statistical Physics, 3rd Edition* (Pergamon Press, Oxford, 1980), Part 1.
- [54] K. Binder, *Introduction to Monte Carlo Methods*, Chapter 5, p. 124, in *Conference Proceedings Vol. 49, Monte Carlo and Molecular Dynamics of Condensed Matter Systems*, K. Binder and G. Ciccotti (Eds.) (SIF, Bologna, 1996).
- [55] M. N. Barber, in *Phase transitions and critical phenomena*, C. Domb and J. L. Lebowitz (Eds.), (Academic, New York, 1983), Vol. 8, p. 146.
- [56] V. Privman (Ed.), *Finite size scaling and numerical simulations of statistical systems* (World Scientific, Singapore, 1990).
- [57] M. E. Fisher and H. Nakanishi, J. Chem. Phys. **75**, 5857 (1981); **78**, 3279 (1983).
- [58] H. Hinrichsen, R. Livi, D. Mukamel, and A. Politi, Phys. Rev. Lett. **79**, 2710 (1997).
- [59] Y. Tu, G. Grinstein, and M. A. Muñoz, Phys. Rev. Lett. **78**, 274 (1997).
- [60] T. Kissinger, A. Kotowicz, O. Kurz, F. Ginelli, and H. Hinrichsen, J. Stat. Mech. P06002 (2005).

- [61] A. Barrat and M. Weigt, Eur. Phys. J. B **13**, 547 (2000).
- [62] M. Gitterman, J. Phys. A: Math. Gen. **33**, 8373 (2000).
- [63] C. M. Bordogna and E. V. Albano, Phys. Rev. Lett. **87**, 118701 (2001).
- [64] C. P. Herrero, Phys. Rev. E **65**, 066110 (2002).
- [65] A. Aleksiejuk, J. A. Hołyst, and D. Stauffer, Physica A **310**, 260 (2002).
- [66] P. Svenson and D. A. Johnston, Phys. Rev. E **65**, 036105 (2002).
- [67] K. Medvedyeva, P. Holme, P. Minnhagen, and B. J. Kim, Phys. Rev. E **67**, 036118 (2003).
- [68] C. P. Herrero, Phys. Rev. E **69**, 067109 (2004).
- [69] D. J. Watts, *Small Worlds* (Princeton University Press, Princeton, 1999).
- [70] R. Albert and A.-L. Barabási, Rev. Mod. Phys. **74**, 47 (2002).
- [71] S. N. Dorogovtsev and J. F. F. Mendes, *Evolution of Networks* (Oxford University Press, New York, 2003).
- [72] M. Newman, A.-L. Barabási, and D. J. Watts (Eds.), *The Structure and Dynamics of Networks* (Princeton University Press, Princeton and Oxford, 2006).
- [73] B. Bollobás and F. R. K. Chung, SIAM J. Discrete Math. **1**, 328 (1988).
- [74] M. E. J. Newman and D. J. Watts, Phys. Rev. E **60**, 7332 (1999).
- [75] A.-L. Barabási and R. Albert, Science **286**, 509 (1999).